TGFβ receptor endocytosis and Smad signaling require synaptojanin1, PI3K–C2α-, and INPP4B-mediated phosphoinositide conversions

Sho Aki[a], Kazuaki Yoshioka[a], Noriko Takuwa[b], and Yoh Takuwa[a,*]
[a]Department of Physiology, Kanazawa University School of Medicine, Kanazawa, Ishikawa 920-8640, Japan;
[b]Department of Health Science, Ishikawa Prefectural University, Kahoku, Ishikawa 929-1210, Japan

ABSTRACT **Phosphoinositide conversion regulates a diverse array of dynamic membrane events including endocytosis. However, it is not well understood which enzymes are involved in phosphoinositide conversions for receptor endocytosis. We found by small interfering RNA (siRNA)-mediated knockdown (KD) that class II PI3K α-isoform (PI3K-C2α), the 5′-phosphatase synaptojanin1 (Synj1), and the 4′-phosphatase INPP4B, but not PI3K-C2β, Synj2, or INPP4A, were required for TGFβ-induced endocytosis of TGFβ receptor. TGFβ induced rapid decreases in PI(4,5)P_2 at the plasma membrane (PM) with increases in PI(4)P, followed by increases in PI(3,4)P_2, in a TGFβ receptor kinase ALK5-dependent manner. TGFβ induced the recruitment of both synaptojanin1 and PI3K-C2α to the PM with their substantial colocalization. Knockdown of synaptojanin1 abolished TGFβ-induced PI(4,5)P_2 decreases and PI(4)P increases. Interestingly, PI3K-C2α KD abolished not only TGFβ-induced PI(3,4)P_2 increases but also TGFβ-induced synaptojanin1 recruitment to the PM, PI(4,5)P_2 decreases, and PI(4)P increases. Finally, the phosphoinositide conversions were necessary for TGFβ-induced activation of Smad2 and Smad3. These observations demonstrate that the sequential phosphoinositide conversions mediated by Synj1, PI3K-C2α, and INPP4B are essential for TGFβ receptor endocytosis and its signaling.**

Monitoring Editor
Carl-Henrik Heldin
Ludwig Institute for Cancer Research

Received: Nov 26, 2019
Revised: Dec 26, 2019
Accepted: Dec 27, 2019

INTRODUCTION

Phosphoinositides, which possess one or more phosphates at the 3-, 4-, and/or 5-OH groups of the inositol ring of phosphatidylinositol (PI), are present in the membrane in relatively small amounts and serve species-specific distinct roles in diverse processes including cell proliferation, cell migration, intracellular trafficking including endocytosis, and cytoskeletal organization (Di Paolo and De Camilli, 2006; Balla, 2013). In clathrin-mediated endocytosis (CME), PI 4,5-bisphosphates (PI(4,5)P_2) is required for the nucleation of clathrin-coated pits (CCPs) (Doherty and McMahon, 2009; Kaksonen and Roux, 2018; Wallroth and Hauke, 2018). The CCPs are maturated and pinched off from the plasma membrane (PM) to become the clathrin-coated vesicles (CCVs), which undergo the fusion with the endosomes. In the endosomes, the major phosphoinositide is PI 3-phosphate (PI(3)P). Thus, phosphoinositides are subjected to the conversion by kinases and phosphatases during the progress of endocytosis (Shin *et al.*, 2005; Billcliff and Lowe, 2014; Marat and Haucke, 2016).

The 3′-phosphorylation of phosphoinositides is catalyzed by three classes of PI 3-kinases (PI3Ks) to generate PI(3)P, PI 3,4-bisphosphates (PI(3,4)P_2), and PI 3,4,5-trisphosphates (PI(3,4,5)P_3) (Bilanges *et al.*, 2019). Class I PI3Ks are activated largely by receptor tyrosine kinases and G protein-coupled receptors to regulate cell proliferation, cell migration, and cell metabolism mainly by generating

This article was published online ahead of print in MBoC in Press (http://www.molbiolcell.org/cgi/doi/10.1091/mbc.E19-11-0662) on January 8, 2020.

*Address correspondence to: Yoh Takuwa (ytakuwa@med.kanazawa-u.ac.jp).

Abbreviations used: BSA, bovine serum albumin; C2α, PI3K-C2α; C2α′, siRNA–resistant PI3K-C2α mutant; C2β, PI3K-C2β; CHC, clathrin heavy chain; CCPs, clathrin–coated pits; CCVs, clathrin–coated vesicles; CME, clathrin–mediated endocytosis; DAPI, 4′, 6-diamidino-2-phenyliindole; EC, endothelial cells; EEA1, early endosome antigen1; EMCCD, electron-multiplying charge-coupled device; HUVEC, human umbilical vein endothelial cells; IB, immunoblotting; INPP4, inositol polyphosphate 4-phosphatases; IP, immunoprecipitation; KD, knockdown; MTMR, myotubularin-related protein; PBS, phosphate-buffered saline; PI, phosphatidylinositol; PI3Ks, phosphatidylinositol 3-kinases; PI(3)P, phosphatidylinositol 3-phosphate; PI(3,4)P_2, phosphatidylinositol 3,4-bisphosphates; PI(3,4,5)P_3, phosphatidylinositol 3,4,5-trisphosphates; PI(4)P, phosphatidylinositol 4-phosphate; PI(4,5)P_2, phosphatidylinositol 4,5-bisphosphates; PLA, proximity ligation assay; PM, plasma membrane; sc-siRNA, scrambled siRNA; SNX, sorting nexin; Synj, synaptojanin.

$PI(3,4,5)P_3$, and class III PI3K Vps34 generates PI(3)P to regulate the autophagic pathway. Class II PI3Ks, which comprise PI3K-C2α (C2α), PI3K-C2β (C2β), and PI3K-C2γ, produce $PI(3,4)P_2$ and PI(3)P (Wallroth and Haucke, 2018; Gulluni *et al.*, 2019). Previous studies (Domin *et al.*, 2000; Gaidarov *et al.*, 2001; Yoshioka *et al.*, 2012; Biswas *et al.*, 2013; Posor *et al.*, 2013; Franco *et al.*, 2014; He *et al.*, 2017) showed that, among class II PI3K members, C2α regulates endocytosis and other membrane traffic events. Posor *et al.* (2013) demonstrated that C2α preferred PI 4-phosphate (PI(4)P) rather than PI as substrate to mainly produce $PI(3,4)P_2$ and that a reduction of $PI(3,4)P_2$ by the overexpression of a phosphoinositide 4′-phosphatase or knockdown (KD) of C2α resulted in inhibition of CME with prolonged maturation of CCPs, indicating an indispensable role of $PI(3,4)P_2$ in CME. Conversely, expression of the mutated hyperactive C2α enhanced $PI(3,4)P_2$ production and endocytosis (Wang *et al.*, 2018). Moreover, they identified the effector molecule of $PI(3,4)P_2$, sorting nexin (SNX)9, which was recruited to CCPs following the accumulation of C2α (Posor *et al.*, 2013; Lo *et al.*, 2017; Schöneberg *et al.*, 2017). Previous studies (Perera *et al.*, 2006; Antonescu *et al.*, 2011) showed that the $PI(4,5)P_2$-specific 5′-phosphatase synaptojanin-1 (Synj1), which converts $PI(4,5)P_2$ to PI(4)P, is recruited to CCPs, suggesting that Synj1 participates in the generation of $PI(3,4)P_2$. Recent studies also showed that the inositol polyphosphate 4-phosphatases (INPPs) negatively regulated signaling through dephosphorylating $PI(3,4)P_2$ (Gewinner *et al.*, 2009; Ivetac *et al.*, 2009). However, the production and breakdown of $PI(3,4)P_2$ in CME were not fully understood.

We recently showed in vascular endothelial cells (EC) that C2α, but not C2β, was required for TGFβ-induced, clathrin-dependent endocytosis of TGFβ receptor serine/threonine kinases and subsequent receptor-mediated phosphorylation of the transcriptional regulators Smad2 and Smad3 (Smad2/3), which occurred in endosomes (Aki *et al.*, 2015). TGFβ induced a rapid increase in the $PI(3,4)P_2$ level at the PM in a C2α-dependent manner in ECs. In the present study, we sought to understand phosphoinositide conversions for the production and breakdown of $PI(3,4)P_2$, the enzymes responsible for conversions, and their requirements in TGFβ-induced receptor endocytosis. We found that TGFβ-induced rise in $PI(3,4)P_2$ required Synj1, which mediated the earliest responses after the addition of TGFβ, that is, $PI(4,5)P_2$ decrease and PI(4)P rise. The 4′-phosphatase INPP4B (Li and Marshall, 2015) seemed to mediate the conversion of $PI(3,4)P_2$ to PI(3)P. Notably, Synj1 and INPP4B, as well as C2α, were essential for TGFβ1-induced receptor endocytosis and Smad2/3 signaling. Furthermore, our data showed that TGFβ induced the rapid colocalization of C2α and Synj1 at the PM and that C2α, as well as Synj1, was required for TGFβ-triggered 5′-dephosphorylation of $PI(4,5)P_2$, suggesting that TGFβ induced the cooperation of Synj1 and C2α. Thus, these data showed an essential role of the phosphoinositide cascade triggered by the cooperating action of Synj1 and C2α for the receptor ligand-induced endocytosis and the following signaling.

RESULTS

Synj1 and INPP4B, as well as C2α, are required for TGFβ1-induced phosphorylation and nuclear translocation of Smad2/3 and TGFβ receptor endocytosis

We first explored the possible involvement of the phosphoinositide-converting enzymes, which relate to the generation and catabolism of the key phosphoinositide, $PI(3,4)P_2$, in TGFβ1-induced Smad signaling. Toward this end, we studied the effects of specific KD of the 5′-specific phosphatases Synj1 and Synj2 that catalyze $PI(4,5)P_2$ conversion to the C2α substrate PI(4)P (Perera *et al.*, 2006), the 4′-specific phosphatases INPP4A and INPP4B that convert $PI(3,4)P_2$ to PI(3)P (Li and Marshall, 2015), and MTMR6 that converts PI(3)P to PI (Maekawa *et al.*, 2014) on TGFβ1-induced receptor endocytosis and Smad signaling in human umbilical vascular EC (HUVEC). Each specific siRNA effectively inhibited the mRNA expression of the respective enzymes but not other enzymes compared with transfection of scrambled small interfering RNA (sc-siRNA) (Figure 1A). We also confirmed that the siRNAs against Synj1, C2α, and INPP4B, for which the antibodies were available, specifically inhibited the expression of the respective proteins (Figure 1B). In sc-siRNA–transfected control HUVECs, TGFβ1 induced increases in Smad2/3 phosphorylation, which reached approximately 8-fold increases over the basal levels at 30 min (Figure 1C). KD of either Synj1 or INPP4B suppressed TGFβ-induced Smad2/3 phosphorylation, like KD of C2α. In contrast, KD of Synj2, INPP4A or MTMR6 did not inhibit phosphorylation of Smad2/3 (Figure 1D). KD of C2α, Synj1, or INPP4B, but not Synj2, INPP4A, or MTMR6, also suppressed TGFβ1-induced nuclear translocation of Smad2/3, as evaluated with anti-Smad2/3 immunofluorescence staining (Figure 1E).

TGFβ1stimulation of sc-siRNA–transfected cells induced a marked reduction in the expression of type I TGFβ receptor ALK5 at the PM with the accumulation of ALK5 in the intracellular compartment, that is, the endocytosis of TGFβ receptor (Figure 2A). TGFβ1stimulation also induced the accumulation of clathrin heavy chain (CHC) at or in the vicinity of the PM in sc-siRNA–transfected cells (Figure 2B). KD of C2α inhibited TGFβ1-induced ALK5 endocytosis (Figure 2A). KD of either Synj1 or INPP4B also inhibited TGFβ1-induced ALK5 endocytosis. In contrast, KD of Synj2, INPP4A, or MTMR6 did not affect TGFβ1-induced ALK5 endocytosis. KD of C2α, Synj1, Synj2, INPP4A, INPP4B, or MTMR6 did not inhibit the accumulation of CHC at the PM (Figure 2B). The proximity ligation assay (PLA) suggested that internalized ALK5 was colocalized with the early endosome marker EEA1 in manners dependent on C2α, Synj1, and INPP4B but not Synj2, INPP4A, or MTMR6 (Figure 2C). The subcellular distribution of anti-early endosome antigen1 (EEA1) signals was not altered by KD of these enzymes (Figure 2D).

Synj1 and C2α are required for TGFβ1-induced rise of $PI(3,4)P_2$

We previously showed that TGFβ1 stimulation induced an acute increase in $PI(3,4)P_2$ at the PM (Aki *et al.*, 2015). We monitored TGFβ-induced changes in $PI(3,4)P_2$ in cells expressing the PI (3,4)P_2-specific fluorescent sensor mCherry-tagged PH^{TAPP1} (He *et al.*, 2017). TGFβ1-induced increase in PI (3,4)P_2 at the PM became detectable within 3–4 min after TGFβ1 addition and maximal approximately at 10 min (Figure 3, A and B). The anti-CHC immunostaining of the cells showed that the mCherry-tagged PH^{TAPP1} signal at the PM of TGFβ1-stimulated cells substantially overlapped with anti-CHC signal (Figure 3A), suggesting that $PI(3,4)P_2$ were increased at the CCPs and/or the CCVs just beneath the PM. KD of C2α but not C2β abolished TGFβ-induced increase in $PI(3,4)P_2$ (Figure 3B and Supplemental Videos S1–S3), suggesting that the rise of $PI(3,4)P_2$ was mediated mainly by C2α. KD of Synj1, which converts $PI(4,5)P_2$ to PI(4)P, also abolished TGFβ1-induced increase in $PI(3,4)P_2$ (Figure 3, A and B). In contrast, KD of INPP4B, which converts $PI(3,4)P_2$ to PI(3)P, did not affect a TGFβ1-induced $PI(3,4)P_2$ increase. Because several previous studies (Bae *et al.*, 2010; Goulden *et al.*, 2019) suggested that $PI(3,4)P_2$ was produced through the 5′-dephosphorylation of $PI(3,4,5)P_3$ generated by class I PI3K in growth factor-stimulated cells, we tested the effect of the class I PI3K-specific inhibitor GDC-0941on GFβ1-induced $PI(3,4)P_2$

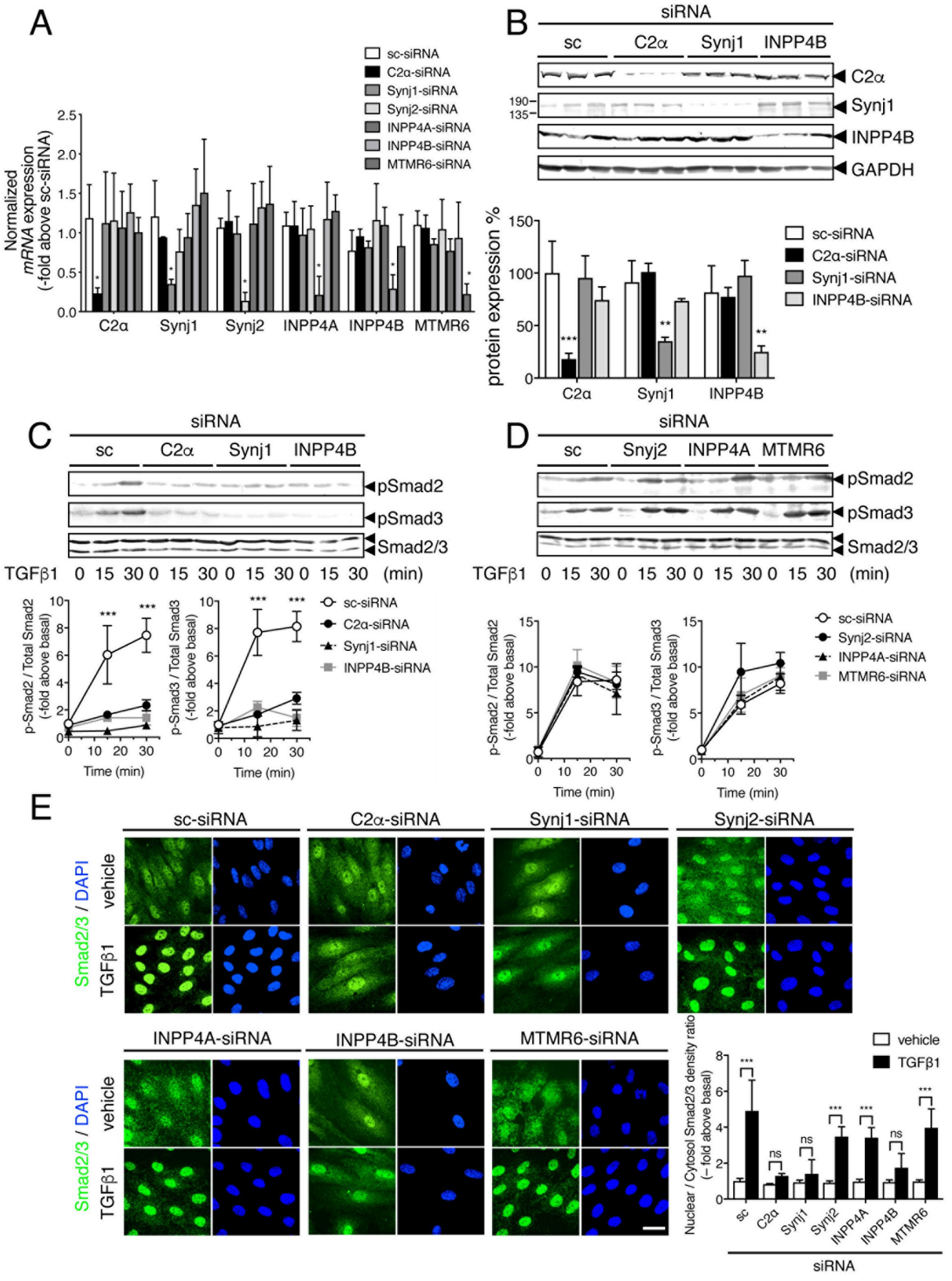

FIGURE 1: Synj1 and INPP4B as well as C2α are required for TGFβ1-induced phosphorylation and nuclear translocation of Smad2/3 in EC. (A) siRNA-mediated KD of the mRNAs of C2α and phosphatases. HUVEC were transfected with scRNA or specific siRNAs against C2α and lipid phosphatases, and the expression of the mRNAs were determined with real-time PCR. (B) siRNA-mediated KD of C2α and phosphatase proteins. HUVEC were transfected with either of the specific siRNAs and sc-siRNA, and the protein expression was analyzed with immunoblotting. Top, representative blots. Bottom, quantified data. (C, D) Time-dependent phosphorylation of Smad2/3 in response to TGFβ1 in C2α- or phosphatase-depleted HUVEC. Cells were transfected with either of the specific siRNAs and sc-siRNA and stimulated with TGFβ1 (5 ng/ml). The cell lysates were subjected to immunoblot analysis using anti-p-Smad2, anti-p-Smad3, and anti-Smad2/3 antibodies. Top, representative blots of Smads. Bottom, quantified data. (E) Immunofluorescence staining of Smad2/3 in TGFβ1-stimulated HUVEC. The cells were transfected with either of the specific siRNAs and sc-siRNA and stimulated with TGFβ1 (5 ng/ml) for 30 min, followed by anti-Smad2/3 antibody immunostaining. ***denotes statistical significance compared with C2a-siRNA, Synj1-siRNA, and INPP4B-siRNA. Nuclei were stained by DAPI. The representative confocal images are shown. Right bottom, quantified data obtained from 48 cells per group. Scale bar, 20 μm.

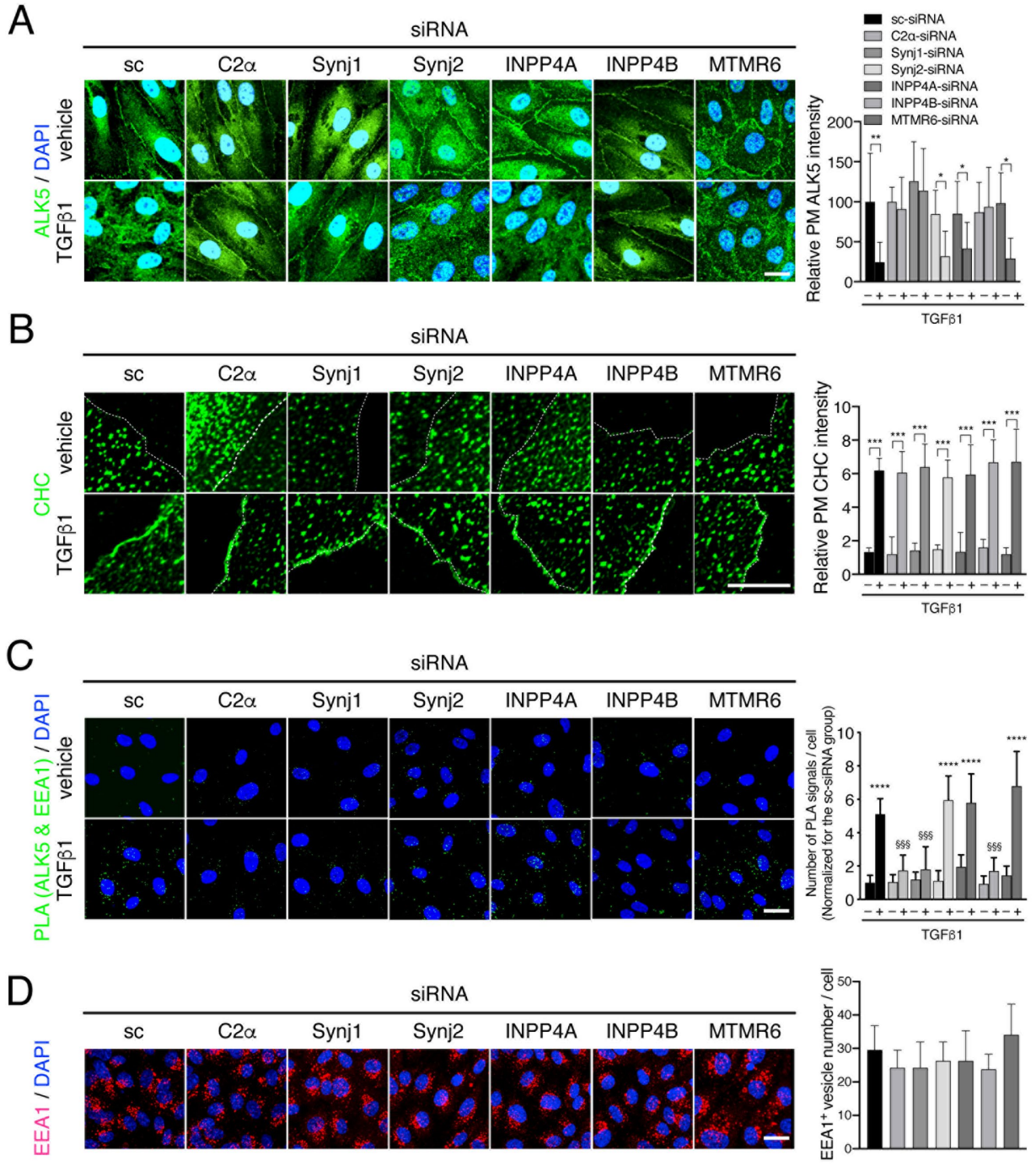

FIGURE 2: Synj1 and INPP4B as well as C2α are required for TGFβ1-induced internalization of TGFβ receptor into early endosomes in EC. (A) Effects of C2α and phosphatase depletion on TGFβ1-induced ALK5 internalization. HUVEC transfected with either of the specific siRNAs and sc-siRNA were stimulated with TGFβ1 (5 ng/ml) for 30 min and subjected to anti-ALK5 immunofluorescence staining. Left, representative confocal images. Scale bar, 20 μm. Right, quantified data of PM ALK5 fluorescence intensities obtained from 24 cells per group. (B) Effects of C2α and phosphatase depletion on clathrin localization. HUVEC transfected with either of the specific siRNAs and sc-siRNA were stimulated with TGFβ1 (5 ng/ml) for 10 min and subjected to anti-CHC immunofluorescence staining. Left, representative confocal images. Scale bar, 20 μm. Right, quantified data of PM CHC immunofluorescence intensities obtained from 24 cells per group. The cell boundaries are indicated in dotted lines. (C) PLA staining of ALK5 and EEA1 (green) in TGFβ1-stimulated HUVEC. Cells transfected with either of the specific siRNAs and sc-siRNA were stimulated with TGFβ1 (5 ng/ml) for 30 min. Left images, PLA staining. Right, quantified data of the PLA signals obtained from 24 cells per group. Nuclei were stained by DAPI. Scale bar, 20 μm. **** and §§§ denote statistical significance compared with TGFb1-nontreated cells in each siRNA-transfected group and TGFb1-treated, sc-siRNA–transfected cells, respectively. (D) Effects of C2α and phosphatase depletion on early endosome. HUVEC transfected with either of the specific siRNAs and sc-siRNA were stained with anti-EEA1 antibody. Left, representative confocal images. Right, quantified data of the anti-EEA1 signals obtained from 24 cells per group. Nuclei were stained by DAPI. Scale bar, 20 μm.

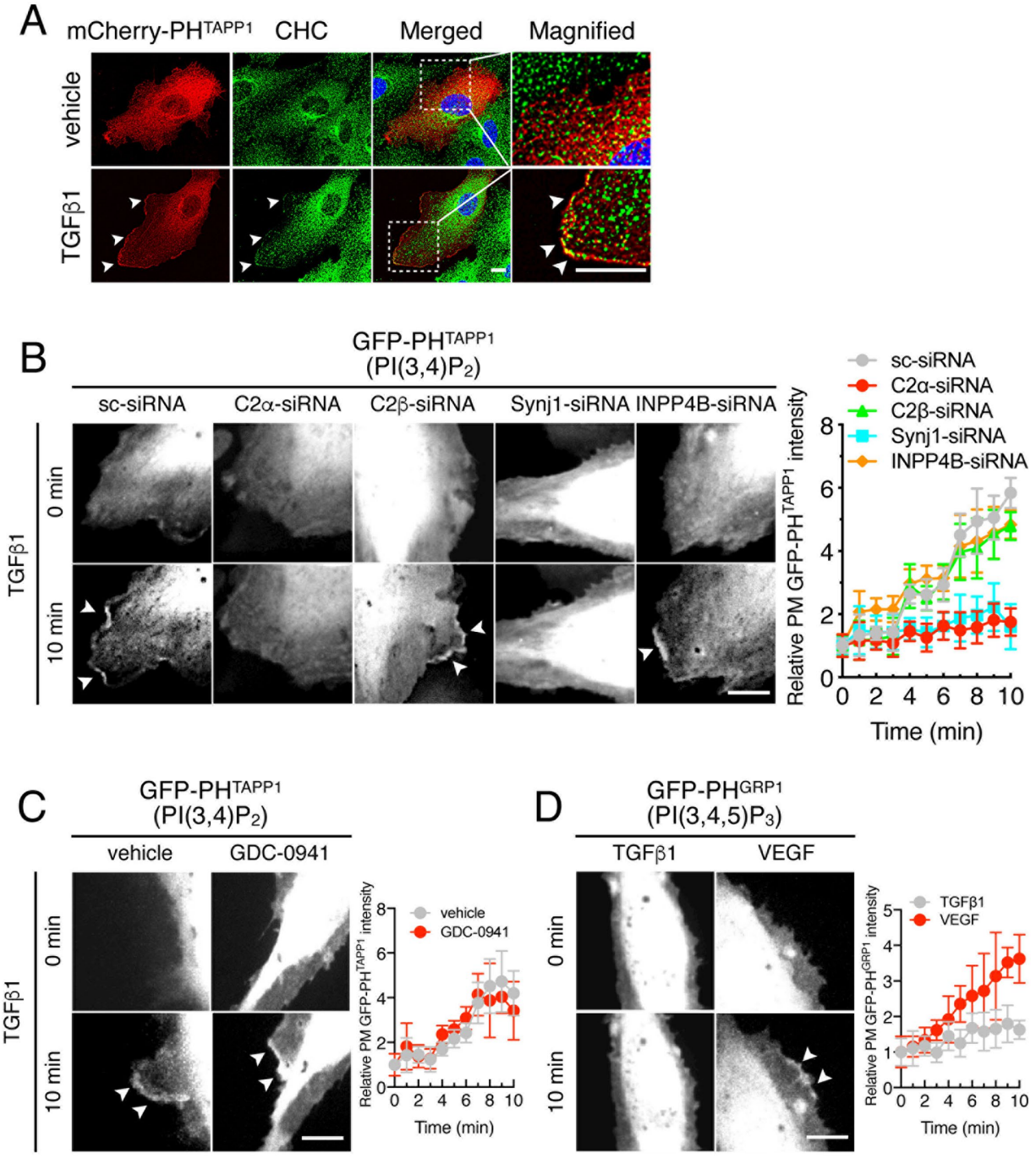

FIGURE 3: Synj1 and C2α are required for TGFβ-induced PI(3,4)P_2 increase at the PM. (A) TGFβ1 induces increases of PI(3,4)P_2 mainly at the clathrin-localized sites of the PM. HUVEC transfected with the PI(3,4)P_2 sensor mCherry-PH^{TAPP1} were stimulated with TGFβ1 (5 ng/ml) for 10 min and subjected to anti-CHC immunofluorescence staining. The extreme right panels are magnified views of the boxed regions. Nuclei were stained by DAPI. The arrowheads denote mCherry-PH^{TAPP1} signals at the anti-CHC-positive PM areas. Nuclei were stained by DAPI. Scale bar, 20 μm. (B) Effects of C2α and phosphatase depletion on TGFβ1-induced PI(3,4)P_2 increase. HUVEC were cotransfected with GFP-PH^{TAPP1} and either of the specific siRNAs and sc-siRNA and stimulated with TGFβ1 (5 ng/ml). The arrowheads in the representative confocal images (left) denote GFP-PH^{TAPP1} signals at the PM. Right, quantified data of the PM GFP-PH^{TAPP1} fluorescence intensities obtained from 24 or 25 cells per group. Scale bar, 20 μm. (C) Effects of the class I PI3K inhibitor GDC-0941 on TGFβ1-induced PI(3,4)P_2 increase. HUVEC transfected with GFP-PH^{TAPP1} were pretreated with GDC-0941 (1 μM) for 30 min and stimulated with TGFβ1 (5 ng/ml) for 10 min. The arrowheads denote mCherry-PH^{TAPP1} signals at the PM. Left, representative confocal images. Scale bar, 20 μm. Right, quantified data of the PM GFP-PH^{TAPP1} fluorescence intensities obtained from 24 cells per group. (D) VEGF but not TGFβ1 induces an increase in PI(3,4,5)P_3 at the PM. HUVEC transfected with GFP-PH^{GRP1} were stimulated with TGFβ1 (5 ng/ml) or VEGF (50 ng/ml) for 10 min. The arrowheads denote GFP-PH^{GRP1} signals at the PM. Left, representative confocal images. Scale bar, 20 μm. Right, quantified data of the PM GFP-PH^{GRP1} fluorescence intensities obtained from 24 cells per group.

increase. GDC-0941 did not inhibit TGFβ1-induced PI(3,4)P_2 increase (Figure 3C), and TGFβ1 did not induce an increase in PI(3,4,5)P_3, which was different from VEGF (Figure 3D). Thus, the 5′-specific phosphatase Synj1 and the C2α, but not the 4′-phosphatase INPP4B or class I PI3K, are required for PI(3,4)P_2 generation in TGFβ1-stimulated HUVEC.

Both Synj1 and C2α are required for TGFβ1-induced PI(4,5)P_2 decrease and PI(4)P increase

Because the 5′-phosphatase Synj1 was required for TGFβ1-induced PI(3,4)P_2 rise (Figure 3B), we explored whether TGFβ1 induced a Synj1-dependent PI(4,5)P_2 conversion to PI(4)P by simultaneously monitoring cellular levels of PI(4,5)P_2 and PI(4)P. In cells coexpressing the PI (4,5)P_2-specific sensor mCherry-PH$^{PLC\delta}$ (Garcia *et al.*, 1995; Lemmon *et al.*, 1995) and the PI(4)P-specific sensor GFP-P4M-SidM (Hammond *et al.*, 2014), TGFβ1 induced a reduction of PI(4,5)P_2 and reciprocal increases of PI(4)P and PI(3,4)P_2 at the PM (Figure 4, A and B). TGFβ1-induced PI(4,5)P_2 reduction and PI(4)P rise occurred rapidly within 10 s after a TGFβ1 addition (Supplemental Videos S4 and S5). We also examined time courses of TGFβ1-induced PI(4)P and PI(3,4)P_2 increases in coexpressing GFP-P4M-SidM and mCherry-tagged PH^{TAPP1}. TGFβ1-induced PI(4)P rise preceded that of PI(3,4)P_2 (Figure 4B). TGFβ1-induced PI(4,5)P_2 reduction and PI(4)P rise were both abolished by KD of Synj1 (Figure 4, C and D, and Supplemental Video S6). These observations together suggested that TGFβ1 induced PI(4,5)P_2 conversion to PI(4)P prior to PI(3,4)P_2 generation through Synj1. Interestingly, TGFβ1-induced PI(4,5)P_2 decrease and PI(4)P rise were also inhibited by C2α KD (Figure 4, C and D, and Supplemental Video S7). TGFβ1-induced PI(4,5)P_2 decrease or PI(4)P rise was not abolished by KD of C2β or INPP4B. These observations suggested that C2α was somehow involved in Synj1-mediated PI(4,5)P_2 hydrolysis.

In contrast to PI(4)P and PI(4,5)P_2, PI(3)P is mainly detected at the intracellular dots, most likely endosomes. TGFβ1 did not change PI(3)P-positive dots in sc-siRNA–transfected cells (Figure 4E). KD of Synj1, C2α, or INPP4B reduced PI(3)P-positive dots in both control and TGFβ1-stimulated cells, suggesting that these enzymes contributed to the endosomal level of PI(3)P. In contrast, the KD of the 3′-phoshatase MTMR6 rather increased PI(3)P-positive dots, suggesting that MTMR6 participated in the dephosphorylation of PI(3)P. Either KD of Vps34 or the class I PI3K inhibitor did not affect PI(3)P-positive dots.

ALK5 mediates TGFβ1-induced triggering of phosphoinositide conversions

TGFβ1 binding to TGFβ receptors activates type I receptor serine/threonine kinases ALK5 or ALK1, resulting in phosphorylation of Smad proteins. To explore the molecular mechanisms underlying TGFβ1-induced phosphoinositide conversion, we tested the effects of the kinase inhibitors of ALK5 and ALK1 on phosphoinositide conversions. The ALK5 kinase-specific inhibitor iALK5 abolished all of the TGFβ1-induced a decrease in PI(4,5)P_2, an increase in PI(4)P, and an increase in PI(3,4)P_2 at the PM (Figure 5, A–C). In contrast, the ALK1 kinase-specific inhibitor iALK1 was without any inhibitory effect on TGFβ1-induced changes in phosphoinositides. These results suggest that TGFβ1-induced phosphoinositide conversions require ALK5 kinase activity.

TGFβ1 induces ALK5-dependent colocalization of Synj1 and C2α at the PM

We explored the mechanism underlying C2α requirement for TGFβ1-induced, Synj1-mediated PI(4,5)P_2 breakdown. In nonstimulated cells that expressed both GFP-tagged C2α (GFP-C2α) and mCherry-tagged Synj1 (mCherry-Synj1), GFP-C2α and mCherry-Synj1 were only marginally localized at the PM and mainly distributed in punctate patterns widely in the intracellular compartment with some overlapping (Figure 6A). TGFβ1 stimulation induced the translocation of GFP-C2α and mCherry-Synj1 to the PM with substantial colocalization (Figure 6A). The immunoprecipitation-Western blot analysis showed that C2α and Synj1 were coprecipitated in sc-siRNA–transfected cells, suggesting that these proteins formed the complex (Figure 6B). Knockdown of Synj1 markedly reduced the amount of the coprecipitated Synj1. TGFβ1 did not enhance the coprecipitation of C2α and Synj1. TGFβ1-induced PM colocalization of GFP-C2α and mCherry-Synj1 was inhibited by iALK5 but not iALK1 (Figure 6C), like TGFβ1-induced changes in PI(4,5)P_2, PI(4)P, and PI(3,4)P_2 at the PM (Figure 5). Interestingly, depletion of C2α abolished TGFβ1-induced recruitment of mCherry-Synj1 to the PM and vice versa (Figure 6, D and E), indicating that the proper PM recruitment of C2α and Synj1 required the existence of the other enzyme. We also studied whether an siRNA-resistant, kinase-deficient C2α mutant, C2α^r (GFP-kdC2α′), could rescue Synj1 translocation in cells depleted of endogenous C2α. In C2α-depleted cells, the expressed C2α-siRNA-resistant wild-type C2α (GFP-wtC2α′) was recruited to the PM together with mCherry-Synj1, whereas in cells cotransfected with GFP-kdC2α^r and mCherry-Synj1, neither protein was recruited to the PM (Figure 6F).

In non–TGFβ-stimulated cells, PI(4,5)P_2 was enriched at the PM, whereas in TGFβ-stimulated cells PI(4,5)P_2 was not enriched at the PM sites where GFP-Synj1 was recruited (Figure 7A). Similarly, in TGFβ-stimulated cells PI(3,4)P_2 was detected at the PM sites where GFP-C2α was recruited (Figure 7B). Moreover, in cells depleted of endogenous C2α, the expression of GFP-wtC2α^r recovered TGFβ1-induced lowering of PI(4,5)P_2 at the PM, whereas that of GFP-kdC2α^r did not (Figure 7C).

These observations together suggest that TGFβ1-induced co-translocation of C2α and Synj1at the PM is dependent on the intact form of C2α and that the phosphoinositide conversion occurs at the PM sites where C2α and Synj1 are recruited.

DISCUSSION

This study demonstrated that TGFβ1 stimulation triggered the conversions of phosphoinositides at the PM of EC via its specific receptor serine/threonine kinase ALK5. TGFβ1 facilitated the conversions of phosphoinositides comprising the 5′-phosphatase Synj1-mediated PI(4,5)P_2 conversion to PI(4)P, the 3′-kinase C2α–mediated PI(4)P conversion to PI(3,4)P_2, and the 4′-phosphatase INPP4B-mediated PI(3,4)P_2 conversion to PI(3)P. Thus, these phosphoinositide conversions likely constitute the sequential conversion cascade. The phosphoinositide cascade was essential for activation of the canonical Smad pathway in TGFβ signaling through its requirement for TGFβ receptor endocytosis. Furthermore, we found that TGFβ1–induced Synj1 recruitment to the PM and Synj1-mediated PI(4,5)P_2 hydrolysis were dependent on C2α, indicating the thus far unrecognized functional cooperation between Synj1 and C2α.

Recent studies (Posor *et al.*, 2013; Schöneberg *et al.*, 2017) showed that PI(3,4)P_2 serves essential roles in the maturation of CCPs in COS-7, HEK293, and HeLa cells under basal nonstimulated conditions. Our study first revealed TGFβ1-triggered phosphoinositide conversions, which led to acute and robust increases in PI(3,4)P_2 at the PM within a few minutes (Figure 3). Second, previous studies (Gewinner *et al.*, 2009; Bae *et al.*, 2010) showed that growth factor stimulation induced an increase in PI(3,4)P_2 via class I PI3Ks. However, TGFβ1-induced PI(3,4)P_2 rise in ECs was mediated by class II

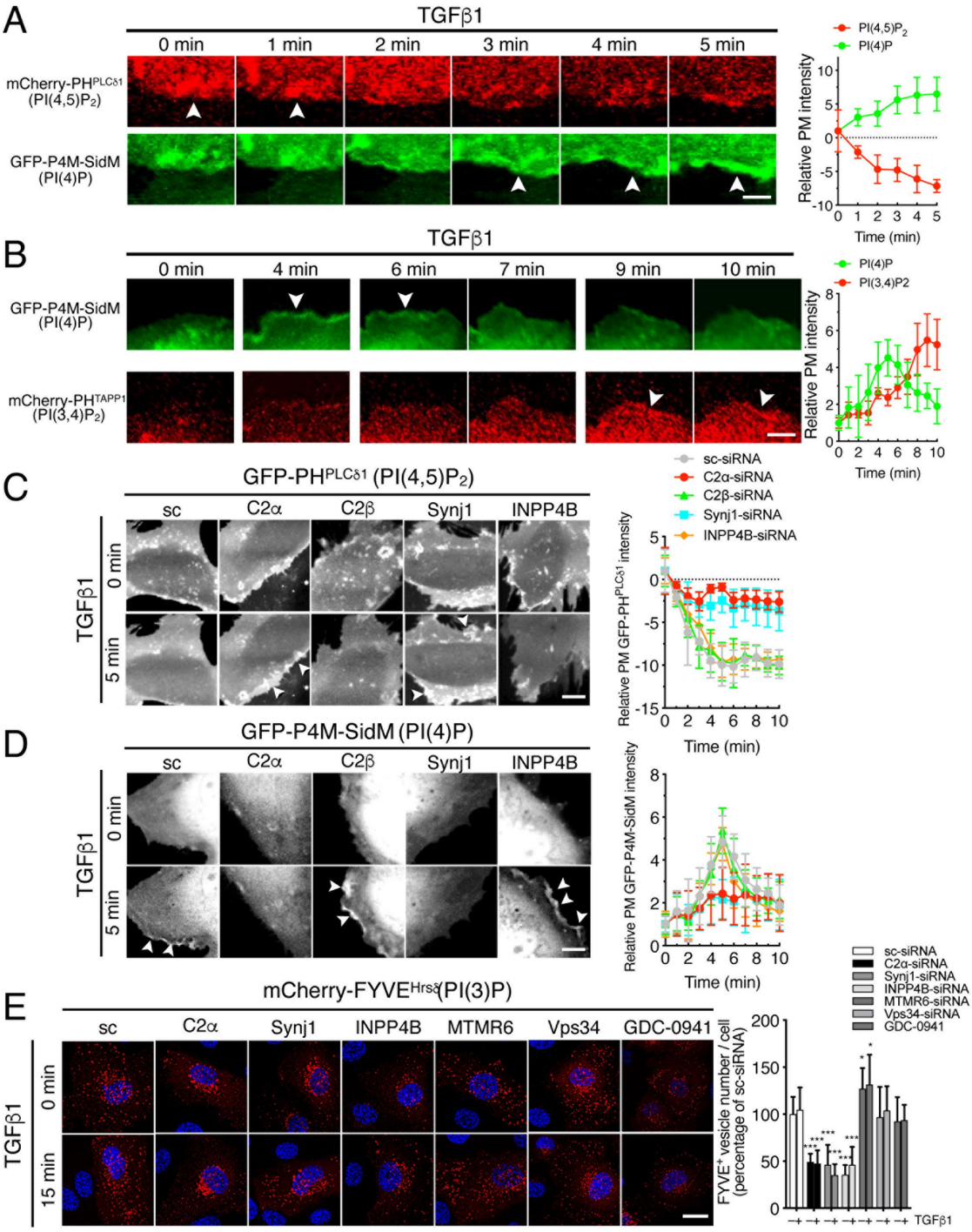

FIGURE 4: Synj1 and C2α are required for TGFβ–induced reduction of PI(4,5)P_2 and rise of PI(4)P. (A) Time-dependent changes in PI(4,5)P_2 and PI(4)P at the PM in TGFβ1-stimulated HUVEC. Cells were cotransfected with mCherry-PH$^{PLC\delta1}$ and GFP-P4M-SidM and stimulated with TGFβ1 (5 ng/ ml) for 5 min. Left, representative confocal images. Scale bar, 20 μm. Right, quantified data of the PM mCherry-PH$^{PLC\delta1}$ or GFP-P4M-SidM fluorescence intensities obtained from 24 cells per group. The arrowheads in the confocal images denote the sites at which PI(4,5)P_2 and PI(4)P levels changed after TGFβ1 stimulation. (B) Time-dependent changes in PI(4)P and PI(3,4)P_2 at the PM in TGFβ1-stimulated HUVEC. Cells were cotransfected with GFP-P4M-SidM and mCherry-PH^{TAPP1} and stimulated with TGFβ1 (5 ng/ml) for 10 min. Left, representative confocal images. Scale bar, 20 μm. Right, quantified data of the PM GFP-P4M-SidM or mCherry-PH^{TAPP1} fluorescence intensities obtained from 24 cells per group. The arrowheads in the confocal images denote the sites in which PI(4)P and PI(3,4)P_2 levels increased after TGFβ1 stimulation. (C) TGFβ1 induces a reduction of PI(4,5)P_2 in manners dependent on Synj1 and C2α but not C2β or INPP4B. HUVEC were cotransfected with GFP-PH$^{PLC\delta1}$ and either of the specific siRNAs and sc-siRNA and stimulated with TGFβ1 (5 ng/ml) for 5 min. Left, representative confocal images. Scale bar, 20 μm. Right, quantified data of the PM GFP-PH$^{PLC\delta1}$ fluorescence intensities obtained from 25 cells per group. The arrowheads in the confocal images denote the sites in which PI(4,5)P_2 level rather increased after TGFβ1 stimulation. (D) TGFβ1 induces a rise of PI(4)P in manners dependent on Synj1 and C2α but not C2β or INPP4B. HUVEC

C2α but not class I PI3K (Figure 3, B and C). Third, TGFβ1 induced a rapid fall of PI(4,5)P_2 with a reciprocal rise of PI(4)P, which was mediated by Synj1 and served as substrate for C2α to generate PI(3,4)P_2. The involvement of Synj1 in CME was consistent with previous reports (Perera *et al.*, 2006; Chang-Ileto *et al.*, 2011). Fourth, the INPP4B was suggested to mediate PI(3,4)P_2 conversion to PI(3)P because the KD of INPP4B reduced cellular PI(3)P level (Figure 4E). These enzymes were essential for TGFβ1-induced TGFβ receptor endocytosis and Smad signaling (Figures 1, C and E, and 2, A and C). Our study unveiled the membrane phosphoinositide dynamics that underlies TGFβ-activated canonical receptor signaling.

The PM PI(4,5)P_2 was converted to PI(3)P through the sequential hydrolysis and phosphorylation in TGFβ1-stimulated cells as mentioned above. PI(3)P was enriched mainly at endosomes (Figure 4E) (Di Paolo and De Camilli, 2006; Marat and Haucke, 2016). The KD of the PI(3)P phosphatase MTMR6 (Hnia *et al.*, 2012; Maekawa *et al.*, 2014) enhanced PI(3)P enrichment in endosomes, suggesting that MTMR6 at least in part contributed to PI(3)P conversion to PI at endosomes. However, MTMR6 KD experiments showed that MTMR6-mediated PI(3)P degradation does not seem to be an important process required for TGFβ receptor endocytosis and subsequent endosomal TGFβ receptor signaling.

In the present study, we unexpectedly found the cooperation of Synj1 and C2α in TGFβ1-stimulated ECs. In nonstimulated cells, fluorescent Synj1 and C2α were colocalized at the dots in the intracellular compartment but not at the PM (Figure 6A), and the immunoprecipitation-Western blot analyses showed that Synj1 and C2α formed the complex (Figure 6B). TGFβ1 stimulation induced the rapid PM recruitment of the enzymes, which needed both Synj1 and C2α, that is, most likely the complex of Synj1 and C2α (Figure 6, D and E). This possibility may also explain why both PI(4,5)P_2 hydrolysis and PI(4)P production required C2α (Figure 4, A and B). The 170-kDa form of Synj1, which possesses the C-terminal tail that contains the binding sites for clathrin, the clathrin adaptor AP-2, and the accessory protein Eps15, is recruited to the CCPs through these binding sites (Perera *et al.*, 2006; Antonescu *et al.*, 2011). C2α also associates with the CCPs through its clathrin-binding domain and PI(4,5)P_2-binding PX-C2 domains (Gaidarov *et al.*, 2001; Wang *et al.*, 2018). Interestingly, TGFβ1-induced recruitment of Synj1 and C2α to the PM was dependent on the kinase activity of ALK5 (Figure 6C), suggesting that protein phosphorylation by ALK5 was involved in the recruitment of Synj1 and C2α complex. Previous studies (Lotti *et al.*, 1996; Okabayashi *et al.*, 1996; Lee *et al.*, 2007) showed that ALK5 phosphorylated the adaptor protein ShcA, which was recruited to a cargo at the CCPs. Therefore, it might be possible that ALK5-mediated phosphorylation of Shc or other proteins promotes the recruitment of Synj1 and C2α complex to the CCPs in the PM much more effectively compared with the recruitment of either alone of Synj1 and C2α. The exact mechanisms of the corecruitment of Synj1 and C2α to the PM and the ALK5 dependence of this process remain to be clarified.

Recent studies (Chen *et al.*, 2018; Wang *et al.*, 2018) showed that C2α becomes fully active by changing its conformation when the N-terminal clathrin-binding domain and the C-terminal PX-C2 domain get contacts with clathrin and membrane PI(4,5)P_2, respectively, at the CCPs. Once C2α is recruited to the CCPs as the complex with Synj1, the production of PI(4)P by Synj1 likely enhances the availability of the substrate PI(4)P to C2α, enabling effective production of PI(3,4)P_2 at the CCPs. It might also be possible that, besides the role as partner for the complex formation, Synj1 might assist the activation of C2α at the CCPs by interacting with C2α.

Our rescue experiments using both wild-type and kinase-deficient forms of C2α showed that, unlike wild-type C2α, the kinase-deficient mutant was not recruited to the PM (Figure 6F). The finding may suggest that the kinase-deficient C2α mutant (D1268A) could not take a conformation that allows for C2α localization at the PM (Wang *et al.*, 2018). Alternatively, PI(3,4)P_2, which was produced by C2α enzymatic activity in collaboration with Synj1, might be required for strengthening the colocalization of Synj1 and C2α at the PM, for example, through recruiting other proteins to the complex. Further studies are required for better understanding the mechanism for TGFβ1-induced recruitment of the Synj1 and C2α complex.

A recent study reported that homozygous loss-of-function mutation of C2α gene results in the phenotype of short stature, coarse facial features, cataract with glaucoma, neurological manifestations including epileptic seizures and stroke, and multiple skeletal abnormalities in children (Tiosano *et al.*, 2019). These patients exhibited compensatory severalfold increases in C2β mRNA expression. A patient with the genetic Synj1 deficiency was also reported to exhibit a severe disorder with neonatal refractory epilepsy and a neurodegenerative disease course (Hardies *et al.*, 2016). Because the brain dominantly expresses the 145-kDa isoform of Synj1 rather than the 170-kDa isoform, a role of Synj1 in vesicle trafficking in the brain may be different from ECs, in which the major Synj1 isoform is 170 kDa. The structure of C-terminal interaction domains is different between 145- and 170-kDa isoforms of Synj1 (Haffner *et al.*, 2000; Perera *et al.*, 2006). Since the present study showed the essential cooperation of Synj1 and C2α, it should be noted that possible functional deficiency of C2α in genetic Synj1-deficient patients and of Synj1 in C2α-deficient patients might contribute to the patient phenotypes. The phenotype of patients with genetic C2α deficiency was also found to have similarities to that of Lowe's syndrome patients caused by loss-of-function mutation of another phosphoinositide 5′-phosphatase OCRL gene (Tiosano *et al.*, 2019). OCRL, which reduces the membrane PI(4,5)P_2 level in the late CCPs and CCVs, is implicated in CME at a little later time point compared with Synj1 (Nakatsu *et al.*, 2010; Kaksonen and Roux, 2018). Therefore, it could be possible that PI(4,5)P_2 accumulation as well as PI(3,4)P_2 deficiency might mechanistically have a contribution to the development of the phenotype of C2α deficiency.

In summary, we unveiled the TGFβ1-activated phosphoinositide conversion cascade, which plays a crucial role in TGFβ-induced CME of TGFβ receptor and, thereby, the canonical TGFβ-induced Smad signaling. The novel cooperative actions of multiple enzymes are involved in the phosphoinositide cascade activation. This

were cotransfected with GFP-P4M-SidM and either of the specific siRNAs and sc-siRNA and stimulated with TGFβ1 (5 ng/ ml) for 5 min. Left, representative confocal images. Scale bar, 20 μm. Right, quantified data of the PM GFP-P4M-SidM fluorescence intensities obtained from 25 cells per group. The arrowheads in the confocal images denote the sites in which PI(4)P level increased after TGFβ1 stimulation. (E) Cellular PI(3)P level is dependent on Synj1, C2α, INPP4B, and MTMR6, but not Vps34. HUVEC were cotransfected with the PI(3)P sensor mCherry-FYVE^{Hrs} and either of the specific siRNAs and sc-siRNA and stimulated with TGFβ1 (5 ng/ml) for 15 min or nontreated. Some dishes were pretreated with GDC-0942 (1 μM) 10 min. Nuclei were stained by DAPI. Left, representative confocal images. Scale bar, 20 μm. Right, quantified data of mCherry-FYVE^{Hrs} fluorescence-positive dot number obtained from 36 cells per group. * and *** denote statistical significance compared with sc-siRNA–transfected cells treated and nontreated with TGFb1.

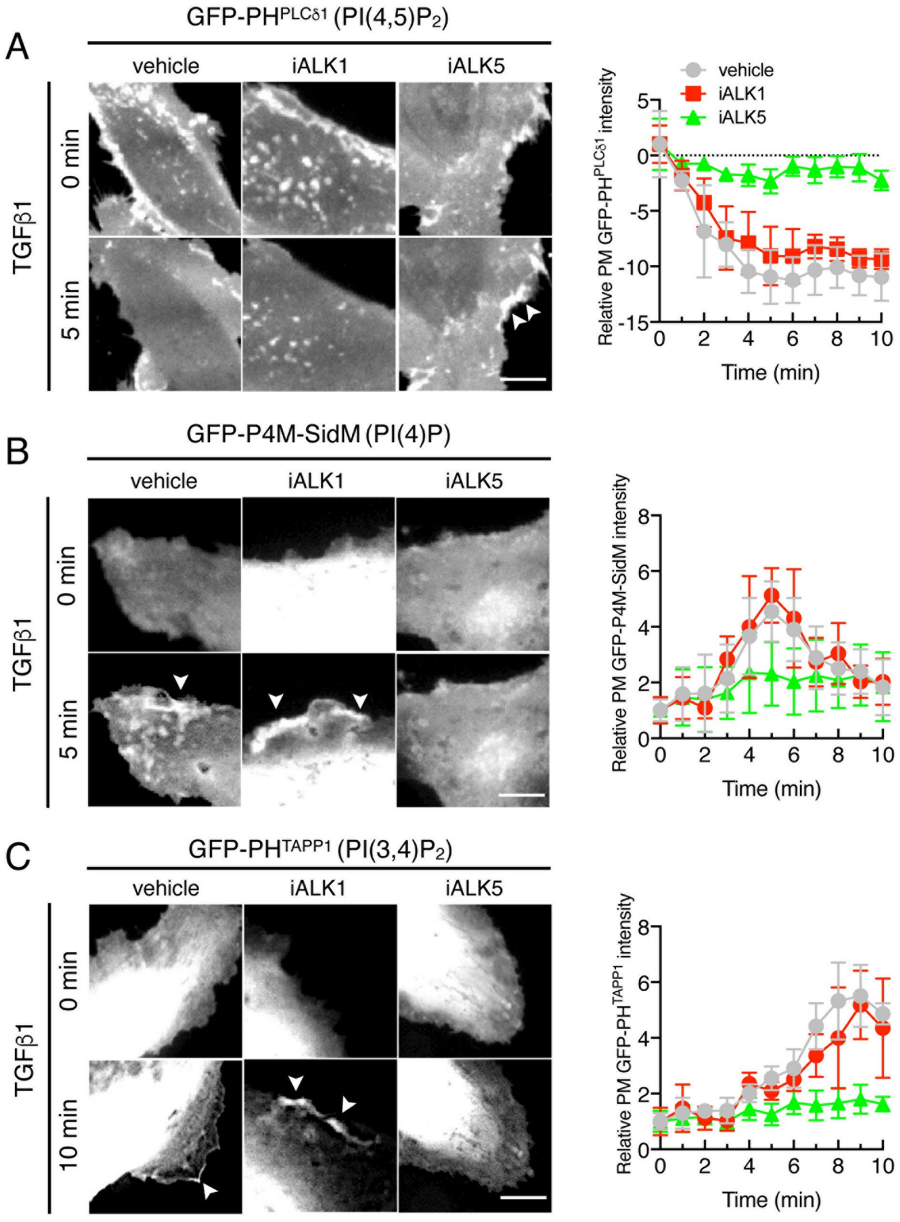

FIGURE 5: TGFβ1-induced phosphoinoitide conversion are mediated by ALK5 but not ALK1. (A–C) Effects of the ALK5 and ALK1 inhibitors on TGFβ-induced reductions of (A) PI(4,5)P2 and rises of (B) PI(4)P and (C) PI(3,4)P_2. HUVEC were transfected with either (A) GFP-PH$^{PLC\delta1}$, (B) GFP-P4M-SidM, or (C) GFP-PH^{TAPP1}. Cells were pretreated with the ALK1 inhibitor iALK1 (LDN193189) (1 μM) or ALK5 inhibitor iALK5 (2-(3-(6-methylpyridin-2-yl)-1H-pyrazol-4-yl)-1,5-naphthyridine) (5 μM) for 30 min and stimulated with TGFβ1 (5 ng/ml) for 5 or 10 min. Representative confocal images at 0 and 5 or 10 min after the additions of TGFβ1 are shown. Left, representative confocal images. Scale bar, 20 μm. Right, quantified data of PM (A) GFP-PH$^{PLC\delta1}$, (B) GFP-P4M-SidM, and (C) GFP-PH^{TAPP1} fluorescence intensities at the PM (24 cells per group).

phosphoinositide cascade may represent a target for treating diseases caused by abnormalities of CME.

MATERIALS AND METHODS

Cells

HUVEC (Lonza) were plated onto type-I collagen-coated (Nitta Gelatin) dishes and flasks and allowed to grow under 5% CO_2 at 37°C in complete endothelial growth medium containing 2% fetal bovine serum and growth factor supplements (EGM-2; #CC3156, Lonza) for HUVECs. HUVECs between passages 4 and 6 were used for all experiments.

Small interfering RNA, plasmids, and transfection

Knockdown of endogenous PI3K isoforms, lipid phosphatases, and Smad4 were performed with the siRNAs that were synthesized using a Silencers siRNA construction kit (#AM1620, Ambion) according to the manufacturer's instruction. The target sequences were: 5′-AAGGTTGGCACTTACAAGAAT-3′ for human PI3K-C2α; 5′-AAGCCGGAAGCTTCTGGGTTT-3′ for human PI3K-C2β 5′-GGGATCTCATCGTGTCCGTATGT-3′ for Synj1; 5′-CGTGAACGGAGGAAAGCAG-3′ for Synj2; 5′-GGCTTTATCATCAAGCTGA-3′ for INPP4A; 5′-ACCTAAGTTTACCAACATGTTAA-3′ for INPP4B; 5′-AAGCACTAAAGGGCTTTCTGT-3′ for MTMR6; HUVECs were transfected with the siRNAs using Lipofectamine 2000 (#11668-019, Invitrogen) before the experiments. The effectiveness of the specific siRNAs was confirmed by the determination of mRNA expression with quantitative PCR (qPCR) and/or Western blotting. The effect of C2β-specific siRNA was previously shown elsewhere (Aung *et al.*, 2018). The expression vector for GFP-C2α was described previously (Aki *et al.*, 2015). The expression vector for GFP-wtC2α^r was generated using a standard PCR-based method (Pham *et al.*, 2018). In C2α^r, the codons AAG-GTT-GGC-ACT-TAC for the amino acids Lys728-Val729-Gly730-Thr731-Tyr732 were replaced by the nucleotides AAA-GTC-GGT-ACC-TAT, which encode the same amino acids. The changes in these nucleotides rendered GFP-wtC2α^r resistant to the C2α-specific siRNA. The kinase-deficient mutant (D1268A) of GFP-C2α was generated using a standard PCR-based method. The expression vectors for GFP-PH^{TAPP1}, GFP-PH$^{PLC\delta}$, and GFP-P4M-SidM were purchased from Addgene. The expression vectors for mCherry-PH^{TAPP1}, mCherry-PH$^{PLC\delta}$, and mCherry-P4M-SidM were provided by Kangmin He (Harvard Medical School). For the expression vector for GFP-Synj1 and mCherry-Synj1, human SYNJ1 cDNA fragments were amplified by PCR using PrimeSTAR HS DNA Polymerase (R010A; Takara-Bio) according to the manufacturer's protocol. The subcloning of the PCR products into pmCherry-C1 (632524; Clontech Laboratories, Mountain View, CA) and pAcGFP1-N vectors (632501; Clontech Laboratories) was performed using the In-Fusion HD Cloning kit (Z9633 N; Clontech Laboratories).

Immunoblotting and immunoprecipitation analysis

At 48 h after siRNA transfection, cells were serum-starved with M199 (Life Technologies) containing 0.5% fatty acid-free bovine serum albumin (BSA) (#A6003, Sigma-Aldrich) for 4 h and then stimulated

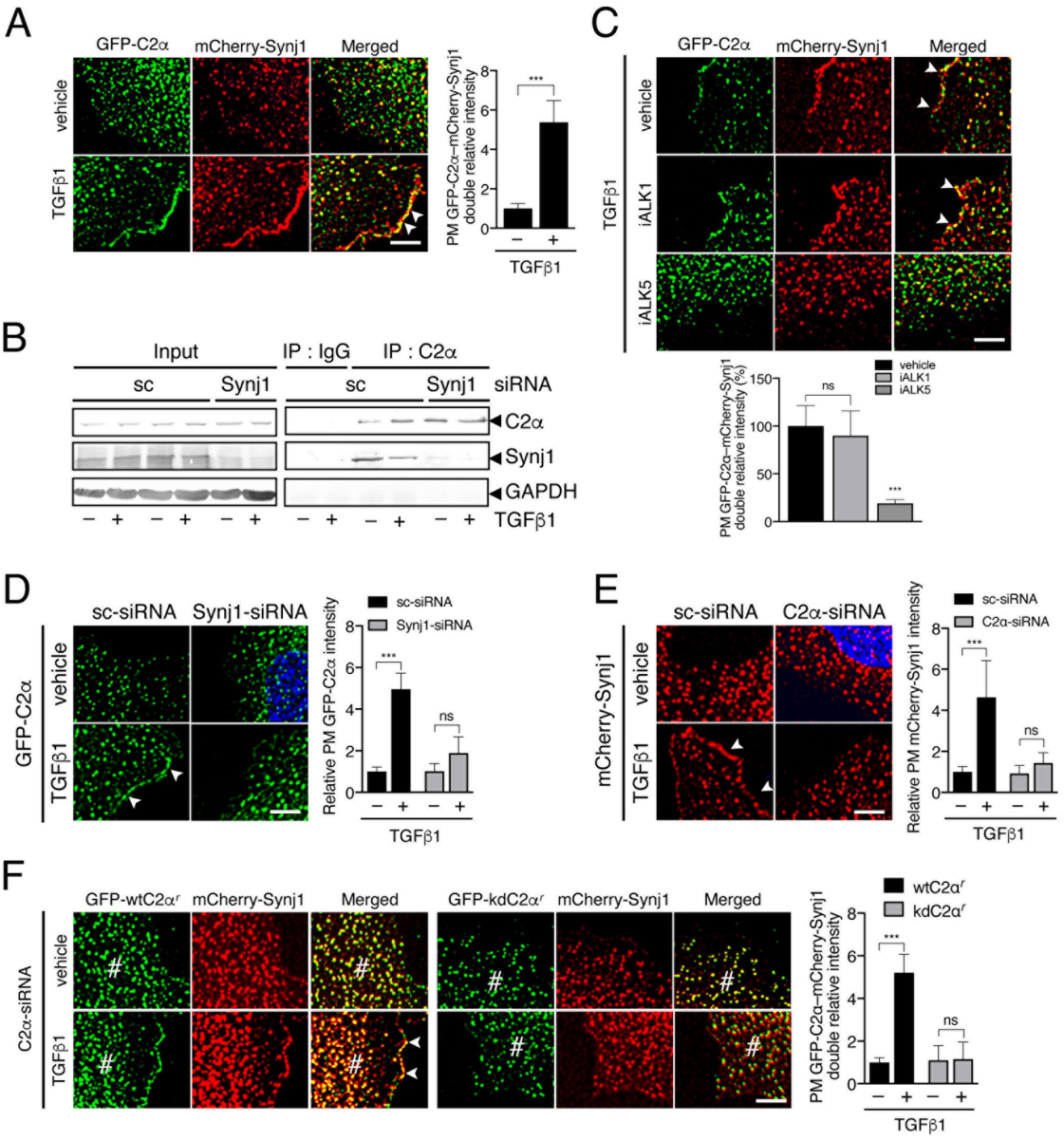

FIGURE 6: TGFβ1 induces ALK5-dependent colocalization of Synj1 and C2α at the PM. (A) TGFβ1 induces the recruitment of GFP-C2α and mCherry-Synj1 to the PM. HUVEC cotransfected with GFP-C2α and mCherry-Synj1 were stimulated with TGFβ1 (5 ng/ml) for 5 min or nontreated. Left, representative confocal images. Scale bar, 10 μm. Right, quantified data of GFP-C2α and mCherry-Synj1 colocalization at the PM (24 cells per group). (B) Coimmunoprecipitation-immunoblotting analysis of C2α and Synj1 in HUVEC. Cells were transfected with sc-siRNA or Synj1-siRNA and stimulated with TGFβ1 (5 ng/ml). Cell lysates were immunoprecipitated (IP) with control-IgG or anti-C2α antibody, followed by immunoblotting (IB) using anti-C2α, anti-Synj1 or anti-GAPDH antibodies. (C) Effects of ALK5 and ALK 1 inhibitors on TGFβ1-induced recruitment of GFP-C2α and mCherry-Synj1 to the PM. Cells cotransfected with GFP-C2α and mCherry-Synj1 were pretreated with iALK1 (1 μM), iALK5 (5 μM), or vehicle for 30 min and then stimulated with TGFβ1 (5 ng/ml) for 5 min. Left, representative confocal images. Scale bar, 10 μm. Right, quantified data of GFP–C2α- and mCherry-Synj1-double positive fluorescence intensities at the PM (24 cells per group). (D) Effects of Synj1 KD on TGFβ1-induced GFP-C2α recruitment to the PM. HUVEC transfected with GFP-C2α and either sc-siRNA or Synj1-siRNA were stimulated with TGFβ1 (5 ng/ml) for 5 min or nontreated. Left, representative confocal images. Scale bar, 10 μm. Right, quantified data of the PM C2α$^+$ fluorescence intensities obtained from 24 cells per group. (E) Effects of C2α KD on TGFβ1-induced mCherry-Synj1 recruitment to the PM. HUVEC transfected with GFP-C2α and either sc-siRNA or C2α-siRNA were stimulated with TGFβ1 (5 ng/ml) for 5 min or nontreated. Left, representative confocal images. Scale bar, 10 μm. Right, quantified data of the PM mCherry-Synj1 fluorescence intensities obtained from 24 cells per group. (F) The expression of wild-type GFP-C2α (GFP-wtC2α^r) but not kinase-deficient GFP-C2α (GFP-kdC2α^r) restores TGFβ1-induced mCherry-Synj1 recruitment to the PM. HUVEC were cotransfected with either GFP- wtC2α^r or GFP-kdC2α^r and either sc-siRNA or C2α-siRNA. Cells were stimulated with TGFβ1 (5 ng/ml) for 5 min. Left, representative confocal images. Scale bar, 10 μm. Right, quantified data of GFP–C2α- and mCherry-Synj1-double positive fluorescence intensities at the PM (24 cells per group).

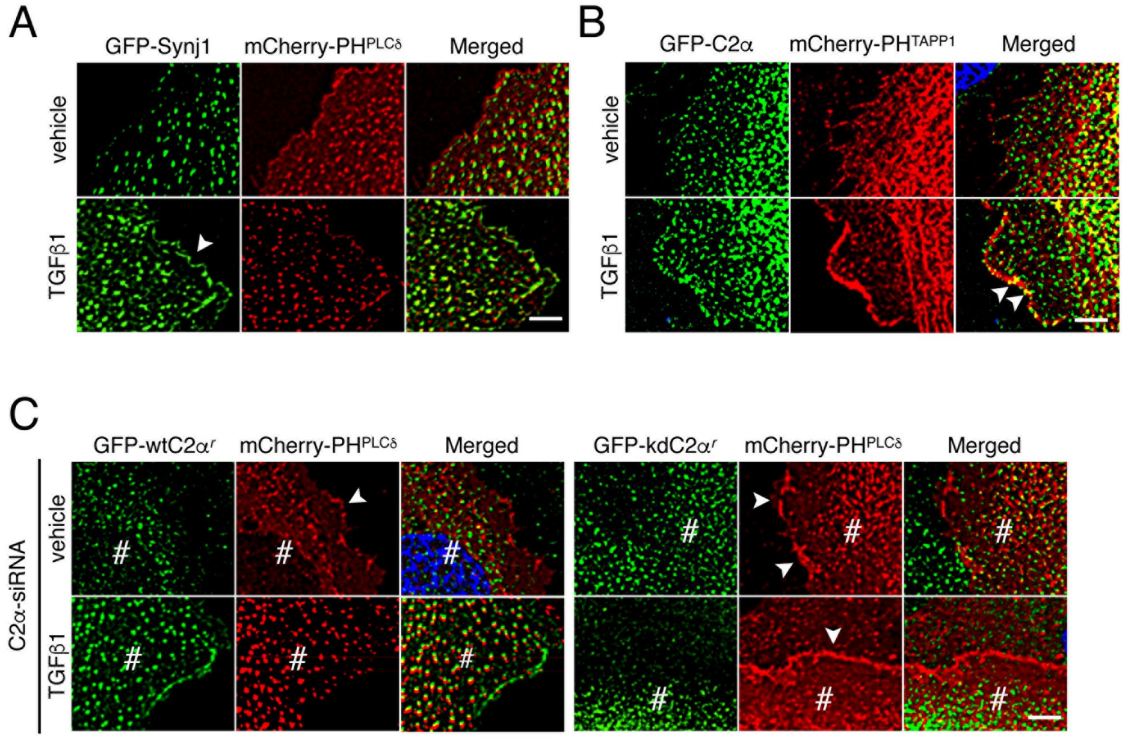

FIGURE 7: TGFβ1-induced PI(4,5)P_2 reduction and PI(3,4)P_2 rise occur with the functional linkage of Synj1 and C2α at the PM sites where these enzymes are recruited. (A) TGFβ induces PI(4,5)P_2 reductions at the PM sites where GFP-Synj1 is recruited. HUVEC were cotransfected with the GFP-Synj1 and mCherry-$PH^{PLC\delta1}$ and stimulated with TGFβ1 (5 ng/ml) for 5 min or nontreated. (B) TGFβ1 induces PI(3,4)P_2 rises at the PM sites where GFP-C2α is recruited. HUVEC were cotransfected with GFP-C2α and mCherry-PH^{TAPP1} and stimulated with TGFβ1 (5 ng/ml) for 10 min or nontreated. (C) The expression of GFP-wtC2α^r but not GFP-kdC2α^r restores TGFβ1-induced PI(4,5)P_2 reductions at the PM. HUVEC were transfected with either GFP-wtC2α^r or GFP-kdC2α^r, mCherry-$PH^{PLC\delta1}$, and C2α-siRNA. Cells were stimulated with TGFβ1 (5 ng/ml) for 5 min. The symbol # denotes the GFP–C2α- and mCherry-$PH^{PLC\delta1}$-cotransfected cells. Nuclei were stained with DAPI (blue). Scale bar, 10 μm.

with TGFβ1 (#100-21, PeproTech). Cells were washed in phosphate-buffered saline (PBS) and lysed in the cell lysis buffer (20 mM Tris-HCl, pH 7.2, 150 mM NaCl, 1 mM $CaCl_2$, 0.5% Triton X-100, 100 mM NaF, 1 mM Na_3VO_4) supplemented with Complete Protease inhibitor cocktail (Roche) by scraping, followed by centrifugation for 15 min at 16, 000 × *g* at 4°C. The resultant supernatants were taken and electrophoresed on 8% SDS–PAGE and transferred onto polyvinylidene difluoride (PVDF) membrane (Millipore). The membranes were blocked in PBS containing 5% BSA and incubated with respective antibodies overnight. The antibodies used are PI3K-C2α (#12402, Cell Signaling); Synj1 (K0130-3, MBL); INPP4B (#8450, Cell Signaling); total Smad2/3 (#610842, BD Bioscience); p-Smad2 (#3101, Cell Signaling); p-Smad3 (#9520, Cell Signaling); ALK5 (sc-398, Santa Cruz); EEA1 (#610456, BD Bioscience); GAPDH (016-25523, Wako). The membranes were incubated with alkaline phosphatase (AP)–conjugated secondary antibodies (anti-mouse immunoglobulin G [IgG] antibody, #7056; anti-rabbit IgG antibody, #7054; Cell Signaling) and visualized by color reaction using 5-bromo-4-chloro-3-indolyl-phosphate/nitro blue tetrazolium (Wako). The band intensities were determined using Image Gauge (Fujifilm). The values were normalized for the value of GAPDH as a loading control and expressed as multiples over the normalized values of nontreated controls. For immunoprecipitation assay, HUVEC lysed in IP buffer (50 mM Tris-HCl, pH 7.5, 150 mM NaCl, 1% NP-40, 0.5% deoxycholate, 0.1% SDS) supplemented with Complete Protease inhibitor cocktails. The lysates were incubated with anti-C2α antibody for 1 h at 4°C with rocking, followed by the incubation with protein G–agarose beads (#1-719-416, Roche) for 1 h at 4°C. After the beads were washed five times, mixed with 2× Laemmli's SDS sample buffer, and boiled. The resultant samples were analyzed with immunoblotting using respective antibodies.

Immunofluorescence staining

HUVECs were plated onto type-I collagen-coated glass bottom dishes (MatTek) and allowed to adhere to dishes in EGM-2 growth medium overnight. Cells were rinsed with prewarmed PBS once and fixed in prewarmed 4% fresh PFA in PBS for 10 min, washed with PBS, and then permeabilized in 0.2% Triton X-100 in PBS for 15 min when necessary. After cells were incubated with 5% normal goat serum for 60 min to inhibit nonspecific protein binding, cells were incubated with mouse monoclonal anti-Smad2/3 antibody, rabbit polyclonal anti-ALK5 antibody or mouse monoclonal anti-CHC antibody (MA1-065, Thermo) for 2 h at room temperature or overnight at 4°C. The cells were incubated for 60 min at room temperature with Alexa Fluor 488–conjugated goat anti-mouse (#A31620, Molecular Probes), Alexa Fluor 488–conjugated goat anti-rabbit (#A11034, Molecular Probes), Alexa Fluor 568–conjugated goat anti-mouse (#A31624, Molecular Probes), or Alexa Fluor 568–conjugated goat anti-rabbit (#A31620, Molecular Probes) secondary antibodies, which were diluted at 1:1000 in PBS. Where appropriate, the cells were counterstained with 4′, 6-diamidino-2-phenyliindole (DAPI; # D1306, Molecular Probe) for 15 min. Cells were mounted on Fluoromount (#K024, Diagnostic BioSystems) and

observed under a custom confocal microscope unit described in detail previously (Yoshioka *et al.*, 2012; Aki *et al.*, 2015; Sarker *et al.*, 2019). The confocal microscopic images shown in Figures 3A, 4C, 6, and 7 were obtained with an inverted Nikon Eclipse Ti2 confocal microscope (Nikon Instruments/ Nikon) equipped with the Perfect Focus System, attached to an Andor Dragonfly spinning-disk unit, Andor electron-multiplying charge-coupled device (EMCCD) camera (iXon DU888; Andor Technology), and a laser unit (Coherent). An oil-immersion objective (PlanApo 60×; NA 1.4; Nikon) was used for all experiments. Excitation for BFP/DAPI, GFP/mEmerald/Alexa 488, and mRFP/mCherry/Alexa 568 and Alexa 647 chromophores was provided by a 405-, 488-, 561-, and 637-nm laser, respectively. Superresolution imaging of fixed cells was performed using an a Dragonfly confocal microscope in super-resolution radial fluctuation Stream mode (Andor Technology).

Live-cell imaging of phosphoinositides

HUVEC that had been transfected with the expression vectors for the phosphoinositide sensors GFP-PH^{TAPP1} ($PI(3,4)P_2$), GFP-$PH^{PLC\delta}$ ($PI(4,5)P_2$), and GFP-P4M-SidM (PI(4)P) were plated on collagen-coated glass-bottomed dishes (MatTek, P35G-1.5-20-C) and allowed to adhere for 16 h before imaging. Cells on a heated stage (37°C; Tokai-Hit) were observed under a custom confocal microscope based on an inverted IX70 microscope (Olympus) equipped with an UPLSAPO × 60/NA1.35-oil objective, a confocal laser unit (CSU10, Yokogawa), an EMCCD digital camera (iXon; Andor), and a Light engine (Lumencor) for three-dimensional time-lapse confocal imaging at a rate of two frames per second. The acquisition and process were controlled by iQ software (Andor). To quantify changes in the fluorescence intensity of sensors at and in the vicinity of the PM, we manually defined all regions of interest that showed fluorescence increases in response to TGFβ1 stimulation in each cell during the observation time period and determined fluorescence intensities with iQ software (Hammond *et al.*, 2012, 2014). The total fluorescence intensity in each cell was normalized by whole-cell fluorescence intensity. For time-lapse data, images were also normalized to the pixel ratio at the baseline level (during a 5-min period before stimulation).

PLA staining

The cells were fixed in prewarmed 4% fresh paraformaldehyde in PBS for 10 min and permeabilized in 0.2% Triton X-100 in PBS for 15 min when necessary. After the cells were incubated with rabbit polyclonal anti-ALK5 antibody and mouse monoclonal anti-EEA1 antibody antibody overnight at 4°C, in situ protein interactions were detected using the Duolink PLA kit according to the manufacturer's instructions (Olink Bioscience).

RNA isolation and quantitative PCR analysis

Total RNA in HUVEC was isolated using TRIzol reagent (Invitrogen). One microgram of total RNA was reverse-transcribed into the first-strand cDNA using QuantiTect RT Kit (#205311; Qiagen). Quantification of gene expression was performed using an ABI-7300 qPCR thermal cycler (Applied Biosystems) in duplicate. The primer sequences were sense: 5′-AGCAAAGGGCTGCGGCTGCT-3′, antisense: 5′-ACCAGAAAGCTCAAGGGGAC-3′ for Synaptojanin2; sense: 5′-GTCCTCTTCAACGTGGGCATCAAT-3′, antisense: 5′-TTTAACCGCACCAAGCTCTCCACA-3′for INPP4A; sense: 5′-GCATTTGACCGAACAGTTTCCAC-3′, antisense: 5′-GCCACAGGGAATAAGTCTTCTCC-3′ for MTMR6. We have validated that these primer pairs are highly specific for each target without cross-amplification. Comparative quantitative analysis was performed using the GeneAmp 7300 system (Applied Bioscience) based on the delta-delta Ct method. The mRNA expression levels were normalized for the expression of GAPDH mRNA, and the results are expressed as multiples over control values.

Statistical analysis

The data are presented as means ± SEM and expressed as the percentages or multiples relative to the values in control cells. Statistical significance was analyzed using Prism 7 software (GraphPad Software). Statistical significance was analyzed either by one-way or two-way analysis of variance followed by Bonferroni's test as appropriate. Results with $p < 0.05$ were considered statistically significant. In all figures, the asterisks indicate statistical significance between the indicated groups at the levels of $p < 0.05$ (*), $p < 0.01$ (**), $p < 0.001$ (***, §§§), and $p < 0.0001$ (****). ns, statistically not significant.

ACKNOWLEDGMENTS

We thank Chiemi Hirose for secretarial assistance. This study was supported by grants from the Japan Society for the Promotion of Science (17K08532 to K.Y., 16K18988 to S.A., 16K15409 to K.I., 17K08542 to N.T., and 15H04673 to Y.T.), by the SENSHIN Medical Research Foundation (K.Y.), and by a Glaxo-Smithkline Research Grant (S.A.). The funders had no role in study design, data collection and analysis, decision to publish, or preparation of the manuscript.

REFERENCES

Aki S, Yoshioka K, Okamoto Y, Takuwa N, Takuwa Y (2015). Phosphatidylinositol 3-kinase class II α-isoform PI3K-C2α is required for transforming growth factor β-induced Smad signaling in endothelial cells. J Biol Chem 290, 6086–6105.

Antonescu CN, Aguet F, Danuser G, Schmid SL (2011). Phosphatidylinositol-(4,5)-bisphosphate regulates clathrin-coated pit initiation, stabilization, and size. Mol Biol Cell 22, 2588–2600.

Aung KT, Yoshioka K, Aki S, Ishimaru K, Takuwa N, Takuwa Y (2018). The class II phosphoinositide 3-kinases PI3K-C2α and PI3K-C2β differentially regulate clathrin-dependent pinocytosis in human vascular endothelial cells. J Physiol Sci 69, 263–280.

Bae YH, Ding Z, Das T, Wells A, Gertler F, Roy P (2010). Profilin1 regulates $PI(3,4)P_2$ and lamellipodin accumulation at the leading edge thus influencing motility of MDA-MB-231 cells. Proc Natl Acad Sci USA 107, 21547–21552.

Balla T (2013). Phosphoinositides: tiny lipids with giant impact on cell regulation. Physiol Rev 93, 1019–1137.

Bilanges B, Posor Y, Vanhaesebroeck B (2019). PI3K isoforms in cell signalling and vesicle trafficking. Nat Rev Mol Cell Biol 9, 515–534.

Billcliff PG, Lowe M (2014). Inositol lipid phosphatases in membrane trafficking and human disease. Biochem J 461, 159–175.

Biswas K, Yoshioka K, Asanuma K, Okamoto Y, Takuwa N, Sasaki T, Takuwa Y (2013). Essential role of class II phosphatidylinositol-3-kinase-C2α in sphingosine 1-phosphate receptor-1-mediated signaling and migration in endothelial cells. J Biol Chem 288, 2325–2339.

Chang-Ileto B, Frere SG, Chan RB, Voronov SV, Roux A, Di Paolo G (2011). Synaptojanin 1-mediated PI(4,5)P2 hydrolysis is modulated by membrane curvature and facilitates membrane fission. Dev Cell 20, 206–218.

Chen KE, Tillu VA, Chandra M, Collins BM (2018). Molecular basis for membrane recruitment by the PX and C2 domains of class II phosphoinositide 3-kinase-C2α. Structure 26, 1612–1625.

Di Paolo G, De Camilli P (2006). Phosphoinositides in cell regulation and membrane dynamics. Nature 443, 651–6577.

Doherty GJ, McMahon HT (2009). Mechanisms of endocytosis. Annu Rev Biochem 78, 857–902.

Domin J, Gaidarov I, Smith ME, Keen JH, Waterfield MD (2000) The class II phosphoinositide 3-kinase PI3K-C2α is concentrated in the trans-Golgi network and present in clathrin-coated vesicles. J Biol Chem 275, 11943–11950.

Franco I, Gulluni F, Campa CC, Costa C, Margaria JP, Ciraolo E, Martini M, Monteyne D, De Luca E, Germena G, *et al.* (2014). PI3K class II α

controls spatially restricted endosomal PtdIns3P and Rab11 activation to promote primary cilium function. Dev Cell 28, 647–658.
Gaidarov I, Smith ME, Domin J, Keen JH (2001). The class II phosphoinositide 3-kinase C2α is activated by clathrin and regulates clathrin-mediated membrane trafficking. Mol Cell 7, 443–449.
Garcia P, Gupta R, Shah S, Morris AJ, Rudge SA, Scarlata S, Petrova V, McLaughlin S, Rebecchi MJ (1995). The pleckstrin homology domain of phospholipase C-δ1 binds with high affinity to phosphatidylinositol 4,5-bisphosphate in bilayer membranes. Biochemistry 34, 16228–16234.
Gewinner C, Wang ZC, Richardson A, Teruya-Feldstein J, Etemadmoghadam D, Bowtell D, Barretina J, Lin WM, Rameh L, Salmena L, *et al*. (2009). Evidence that inositol polyphosphate 4-phosphatase type II is a tumor suppressor that inhibits PI3K signaling. Cancer Cell 16, 115–125.
Goulden BD, Pacheco J, Dull A, Zewe JP, Deiters A, Hammond GRV (2019). A high avidity biosensor reveals PI(3,4)P_2 is predominantly a class I PI3K signaling product. J Cell Biol 218, 1066–1079.
Gulluni F, De Santis MC, Margaria JP, Martini M, Hirsch E (2019). Class II PI3K functions in cell biology and disease. Trends Cell Biol 29, 339–359.
Haffner C, Di Paolo G, Rosenthal JA, de Camilli P (2000). Direct interaction of the 170 kDa isoform of synaptojanin 1 with clathrin and with the clathrin adaptor AP-2. Curr Biol 10, 471–474.
Hammond GR, Fischer MJ, Anderson KE, Holdich J, Koteci A, Balla T, Irvine RF (2012) PI4P and PI(4,5)P2 are essential but independent lipid determinants of membrane identity. Science 337, 727–730.
Hammond GR, Machner MP, Balla T (2014) A novel probe for phosphatidylinositol 4-phosphate reveals multiple pools beyond the Golgi. J Cell Biol 205, 113–126.
Hardies K, Cai Y, Jardel C, Jansen AC, Cao M, May P, Djémié T, Hachon Le Camus C, Keymolen K, *et al*. (2016). Loss of SYNJ1 dual phosphatase activity leads to early onset refractory seizures and progressive neurological decline. Brain 139, 2420–2430.
He K, Marsland R III, Upadhyayula S, Song E, Dang S, Capraro BR, Wang W, Skillern W, Gaudin R, Ma M, Kirchhausen T (2017). Dynamics of phosphoinositide conversion in clathrin-mediated endocytic traffic. Nature 552, 410–414.
Hnia K, Vaccari I, Bolino A, Laporte J (2012). Myotubularin phosphoinositide phosphatase: cellular functions and disease pathophysiology. Trends Mol Med 18, 317—327.
Ivetac I, Gurung R, Hakim S, Horan KA, Sheffield DA, Binge LC, Majerus PW, Tiganis T, Mitchell CA (2009). Regulation of PI(3)K/Akt signalling and cellular transformation by inositol polyphosphate 4-phosphatase-1. EMBO Rep 10, 487–493.
Kaksonen M, Roux A (2018). Mechanisms of clathrin-mediated endocytosis. Nat Rev Mol Cell Biol 19, 313–326.
Lee MK, Pardoux C, Hall MC, Lee PS, Warburton D, Qing J, Smith SM, Derynck R (2007). TGF-β activates Erk MAP kinase signalling through direct phosphorylation of ShcA. EMBO J 26, 3957–3967.
Lemmon MA, Ferguson KM, O'Brien R, Sigler PB, Schlessinger J (1995) Specific and high-affinity binding of inositol phosphates to an isolated pleckstrin homology domain. Proc Natl Acad Sci USA 92, 10472–10476.
Li H, Marshall AJ (2015). Phosphatidylinositol (3,4) bisphosphate-specific phosphatases and effector proteins: A distinct branch of PI3K signaling. Cell Signal 27, 1789–1798.
Lo WT, Vujičić Žagar A, Gerth F, Lehmann M, Puchkov D, Krylova O, Freund C, Scapozza L, Vadas O, Haucke V (2017). A coincidence detection mechanism controls PX-BAR domain-mediated endocytic membrane remodeling via an allosteric structural switch. Dev Cell 43, 522–529.
Lotti LV, Lanfrancone L, Migliaccio E, Zompetta C, Pelicci G, Salcini AE, Falini B, Pelicci PG, Torrisi MR (1996). Sch proteins are localized on endoplasmic reticulum membranes and are redistributed after tyrosine kinase receptor activation. Mol Cell Biol 16, 1946–1954.
Maekawa M, Terasaka S, Mochizuki Y, Kawai K, Ikeda Y, Araki N, Skolnik EY, Taguchi T, Arai H (2014). Sequential breakdown of 3-phosphorylated phosphoinositides is essential for the completion of micropinocytosis. Proc Natl Acad Sci USA 111, E978–E987.
Marat AL, Haucke V (2016). Phosphatidylinositol 3-phosphates-at the interface between cell signalling and membrane traffic. EMBO J 35, 561–579.
Nakatsu F, Perera RM, Lucast L, Zoncu R, Domin J, Gertler FB, Toomre D, De Camilli P (2010). The inositol 5-phosphatase SHIP2 regulates endocytic clathrin-coated pit dynamics. J Cell Biol 190, 307–315.
Okabayashi Y, Sugimoto Y, Totty NF, Hsuan J, Kido Y, Sakaguchi K, Gout I, Waterfield MD, Kasuga M (1996). Interaction of Shc with adaptor protein adaptins. J Biol Chem 271, 5265–5269.
Perera RM, Zoncu R, Lucast L, De Camilli P, Toomre D (2006). Two synaptojanin 1 isoforms are recruited to clathrin-coated pits at different stages. Proc Natl Acad Sci USA 103, 19332–19337.
Pham HQ, Yoshioka K, Mohri H, Nakata H, Aki S, Ishimaru K, Takuwa N, Takuwa Y (2018). MTMR4, a phosphoinositide-specific 3′-phosphatase, regulates TFEB activity and the endocytic and autophagic pathways. Genes Cells 23, 670–687.
Posor Y, Eichhorn-Gruenig M, Puchkov D, Schöneberg J, Ullrich A, Lampe A, Müller R, Zarbakhsh S, Gulluni F, Hirsch E, *et al*. (2013). Spatiotemporal control of endocytosis by phosphatidylinositol-3,4- bisphosphate. Nature 499, 233–237.
Sarker MAK, Aki S, Yoshioka K, Kuno K, Okamoto Y, Ishimaru K, Takuwa N, Takuwa Y (2019). Class II PI3Ks α and β are required for Rho-dependent uterine smooth muscle contraction and parturition in mice. Endocrinology 160, 235–248.
Schöneberg J, Lehmann M, Ullrich A, Posor Y, Lo WT, Lichtner G, Schmoranzer J, Haucke V, Noé F (2017). Lipid-mediated PX-BAR domain recruitment couples local membrane constriction to endocytic vesicle fission. Nat Commun 8, 15873.
Shin HW, Hayashi M, Christoforidis S, Lacas-Gervais S, Hoepfner S, Wenk MR, Modregger J, Uttenweiler-Joseph S, Wilm M, Nystuen A, *et al*. (2005). An enzymatic cascade of Rab5 effectors regulates phosphoinositide turnover in the endocytic pathway. J Cell Biol 170, 607–618.
Tiosano D, Baris HN, Chen A, Hitzert MM, Schueler M, Gulluni F, Wiesener A, Bergua A, Mory A, Copeland B, *et al*. (2019). Mutations in PIK3C2A cause syndromic short stature, skeletal abnormalities, and cataracts associated with ciliary dysfunction. PLoS Genet 15, e1008088.
Wallroth A, Haucke V (2018). Phosphoinositide conversion in endocytosis and the endolysosomal system. J Biol Chem 293, 1526–1535.
Wang H, Lo WT, Vujičić Žagar A, Gulluni F, Lehmann M, Scapozza L, Haucke V, Vadas O (2018). Autoregulation of class II Alpha PI3K activity by its lipid-binding PX-C2 domain module. Mol Cell 71, 343–351.
Yoshioka K, Yoshida K, Cui H, Wakayama T, Takuwa N, Okamoto Y, Du W, Qi X, Asanuma K, Sugihara K, *et al*. (2012). Endothelial PI3K-C2α, a class II PI3K, has an essential role in angiogenesis and vascular barrier function. Nat Med 18, 1560–1569.